

AN INDUCTIVE SELF-COMPLEMENTARY HILBERT-CURVE ANTENNA FOR UHF RFID BROADBAND AND CIRCULAR POLARIZATION TAGS

J. C. Liu

Department of Electrical Engineering
Ching Yun University
Chung-Li, Tao-yuan, Taiwan 32097, R.O.C.

B. H. Zeng

Department of Communication Engineering
Yuan Ze University
Chung-Li, Tao-yuan, Taiwan 32003, R.O.C.

I. Chen

Identification and Security Technology Center
Industrial Technology Research Institute
Hsinchu, Taiwan, R.O.C.

C. C. Chang

Department of Computer and Communication Engineering
China University of Technology
Hukou, Hsinchu, Taiwan, R.O.C.

D. C. Chang

Department of Communication Engineering
Yuan Ze University and Oriental Institute of Technology
Taiwan, R.O.C.

Abstract—A novel fractal tag antenna constructed with Hilbert-curve and self-complementary configuration is proposed for UHF RFID applications. The main aim of this paper is to merge the meander line and meandered-slot structure of the RFID tag antenna in order to obtain a good performance of compact, broadband, circular polarization and conjugate impedance matching. The tunable inductive and broadband (-10 dB BW = 115 MHz) characteristics

of frequency responses and directivity (1.62 dBi) as well as circular polarization (-3 dB AR BW = 315 MHz) of radiation patterns for 900 MHz are studied and presented.

1. INTRODUCTION

Recently there has been a rapidly growing interest in RFID systems and its applications. Operating frequencies including 125–134 kHz and 140–148.5 kHz LF band, 13.56 MHz HF band and 868–960 MHz UHF band were applied to various supply chains. 433 MHz band was decided for active reader and 2.45 GHz band was applied for WiFi reader. Besides the reader antennas, the requirements of tag antennas are necessary for applications. In which, due to the benefit of long read range and low cost, the UHF tag will be used as the system of distribution and logistics around the world [2–19].

Meander line antennas were commonly for UHF tags, due to the characteristics of high gain, omni-directionality, planarity and relatively small surface size [6]. However, the length-to-width ratio limited as 5 : 1 was proposed [3]. Recently, the half-Sierpinski fractal antenna was introduced with a small length-to-width ratio ($< 2 : 1$) [12]. The inductive impedance of tag antenna was necessary for matching the capacitive terminations of chip IC, thus the tuning apparatus was proposed [5, 9–11, 18]. H-shaped meandered-slot antennas with the performance of broadband and conjugate impedance matching were developed for on-body applications [15, 16]. The ceramic patch antenna mountable on metallic objects was proposed [17]. The compact microstrip antenna with Koch curve was presented [19]. On the other hand, the self-complementary dipoles were introduced for the performance of wideband, high impedance and balun [20–27].

The Hilbert-curve, was known as the space-filling curves [28]. The structure of this shape can be made of a long metallic wire compacted within a patch. As the iteration order of the curve increases, the Hilbert-curve can be space-filling the patch. It has been used in fractal antenna with size reduction [29–31].

The main aim of this paper is to merge the meander line and meandered-slot structure of the RFID tag antenna in order to obtain a good performance of compact, broadband and conjugate impedance matching. Meantime, demonstrating the performance with a self-complementary Hilbert-curve tag antenna is proposed. The self-complementary Hilbert-curve tag antenna is constructed with substrate, Hilbert-curve, Hilbert-curve slot and tuning pad. For

circular polarization analysis, the current distribution and electric field are exhibited. The inductive and broadband characteristics of frequency responses and directivity feature of radiation patterns and polarization are studied and presented.

2. ANTENNA CONFIGURATION AND BASIS

2.1. UHF RFID Meander-line Antenna

The typical dipole antenna consists of two parts, in Fig. 1, one is the dipole resonators with half-wavelength for resonance and the other is the balun for the impedance transfer of balance to unbalance terminations. The standing voltage and current distribute among the dipole with maxima current and minimum voltage feeding in the center (0°) for linear polarization. The principle mode (#1) waves are radiated toward the broadside. For size reduction, in Fig. 2, the meander-line configuration was applied in tag antenna. By tuning load-line structure, more wideband and inductive performance can be achieved.

2.2. Self-complementary Hilbert-curve Tag Antenna

Complementary Hilbert-curve tag antenna is constructed with substrate, Hilbert-curve, Hilbert-curve slot and tuning pad in Fig. 3. The Hilbert-curve is consisted of three series Hilbert-curve with the 3rd iteration. The dimensions are $L_1 = 23.5$ mm, $L_2 = 24$ mm, $L_t = 5$ mm, $L_f = 1.5$ mm, $W_1 = 7.5$ mm, $W_2 = 8.5$ mm, $W_3 = 0.75$ mm, $W_4 = 0.5$ mm, and $g = 0.35$ mm. The thicknesses of RT/duroid-6010 substrate are h_1 is 1.27 mm and the relative permittivity ϵ_{r1} is 10.2 shown in Fig. 4. The total length of series Hilbert-curve

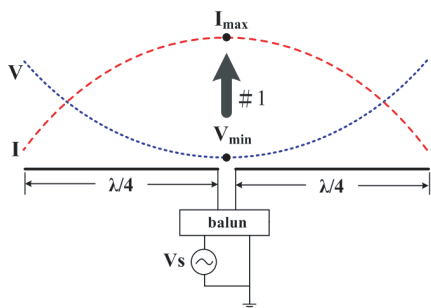


Figure 1. Dipole antenna.

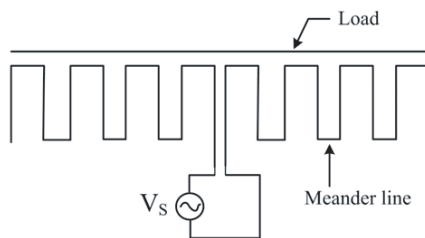


Figure 2. Meander line antennas.

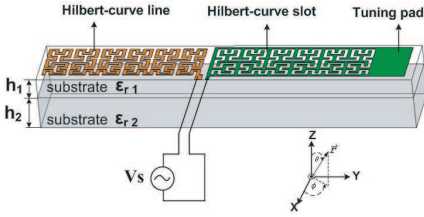


Figure 3. Self-complementary Hilbert-curve tag antenna.

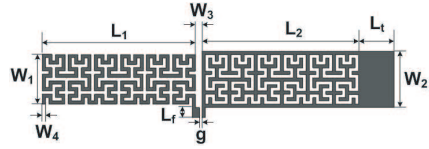


Figure 4. Dimensions of self-complementary Hilbert-curve tag antenna.

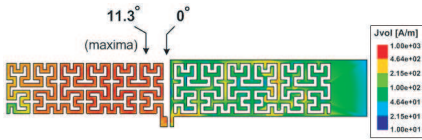


Figure 5. Current distributions.

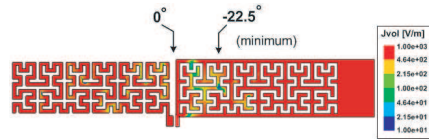


Figure 6. Electric fields.

is 189 mm, it can built a $\lambda_0/2$ resonance of the desired frequency 900 MHz. Conventional tags are design in free space but when on-body applications are required [15], the features caused by additional subjects need to be take into account in the design. In Fig. 4, the on-body configuration also propose the design for finite-thickness ($\epsilon_{r2} = 10.5$, $h_2 = 5.08$ mm) subject and even in this case a good impedance matching is achieved.

Circular polarization wave can be generated by exciting two orthogonal modes in a patch, these two orthogonal modes are in 90-degree phase with the sign of the relative phase determining polarization hand. The orthogonal modes may be excited in a number of ways, which include orthogonal feeds, orthogonal patches, multiple feeds and truncated-corner patches [1].

Figure 5 illustrates the simulated current distributions and Fig. 6 depicts the simulated electric fields among the planar structures, which provide a clearly physical insight on understanding the circular polarization of the proposed antenna. Fig. 5 shows that the Hilbert-curve is excited with concentrating current distributions at the 900 MHz resonance while the maximum amplitude located at the left arm with 11.3° deviation from central feed-line (0°). The Hilbert-curve slot is expressed with lower current distributions. Fig. 6 presents both Hilbert-curve line and Hilbert-curve slot are excited with intensive electric fields at the 900 MHz resonance while the minimum amplitude presented at the right arm with -22.5° deviation. Obviously, the

second mode (#2) waves are radiated along the arms and toward the end-fire. Since the second mode (#2) waves among the two arms of the Y -axis occur, in company with the inherent principle mode (#1) waves toward the broadside of the Z -axis exist, the necessary two orthogonal modes in the antenna can be obtained in Fig. 7. Meantime, these two mode resonances are with 33.8° phase difference. Thus, the circular polarization can be observed along a certain direction of X -axis ($\phi = 0^\circ$ and $\theta = 90^\circ$). It can be observed in Fig. 11.

The maximum activation distance of the tag for the given frequency is given [15, 16] by

$$d_{\max} = \frac{c}{4\pi f} \sqrt{\frac{EIRP_R}{P_{chip}} \tau G} \tag{1}$$

where $EIRP_R$ is the effective transmitted power of reader, P_{chip} is the sensitivity of tag microchip, G is the maximum tag antenna gain, and the power transmission factor

$$\tau = \frac{4R_{chip}R_A}{|Z_{chip} + Z_A|^2} \leq 1 \tag{2}$$

with tag antenna impedance ($Z_A = R_A + jZ_A$) and microchip impedance ($Z_{chip} = R_{chip} + jZ_{chip}$).

3. SIMULATIONS AND RESULTS

By using the commercial software of HFSS tool [32], the simulation results included return loss spectrums, impedance spectrum, circular

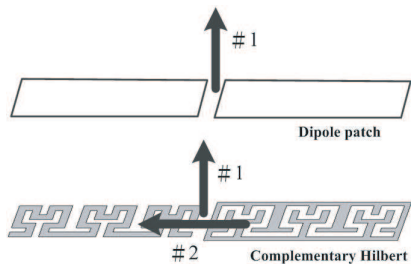


Figure 7. Orthogonal modes.

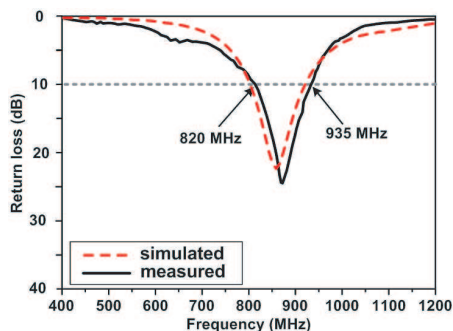


Figure 8. Simulated and measured results of return loss spectrum.

polarization and two-cut radiation patterns are presented and analyzed. For comparison, the return loss spectrums of the proposed antenna with UHF-bands of 900 MHz are measured and simulated shown in Fig. 8.

The simulated and measured results of frequency responses are in agreement. In measurement, while the return loss is smaller than -10 dB, the frequency responses cover both Europe 865.6–867.6 MHz band and USA 902–928 MHz band, ranging from 820 to 935 MHz (bandwidth = 115 MHz). For applications, the frequency responses are fully applied in the operation bands of the RFID UHF-band. For impedance spectrum analysis in Fig. 9, it shows the real parts of impedance become maximum value (178.7Ω) at 970 MHz frequency, the real parts of impedance value (102.5Ω) and the imaginary parts of impedance present inductive characteristic ($+41.3 \Omega$) at 900 MHz frequency. The inductive impedance can be available for matching the capacitive RFID chip. A $0.127\lambda_0$ shifted line with $0.131\lambda_0$ short-circuit stub is inserted for matching the 50Ω termination of the network analyzer.

The radiation patterns are obtained by an automatic measurement system in an anechoic chamber. The under-tested antenna is located on the X - Y plane shown in Fig. 3, and the feeding line is located along the X -axis. Thus, two radiation patterns with Y - Z cut and X - Z cut are obtained. The two cut patterns with resonant 900 MHz are represented in Fig. 10 respectively. The X - Z cut express the patterns as $\phi = 0^\circ$ and θ varied and the Y - Z cut depict the patterns as $\phi = 90^\circ$ and θ varied. Conical patterns are observed at broadside in the Y - Z cut and quasi-omnidirectional patterns are obtained in the X - Z cut. The

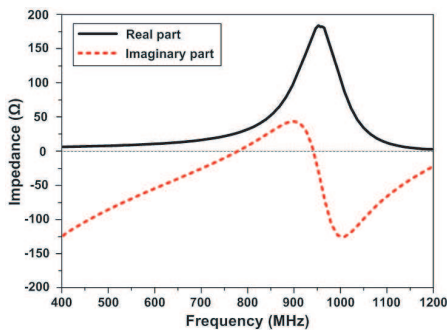


Figure 9. Simulated results of impedance spectrum.

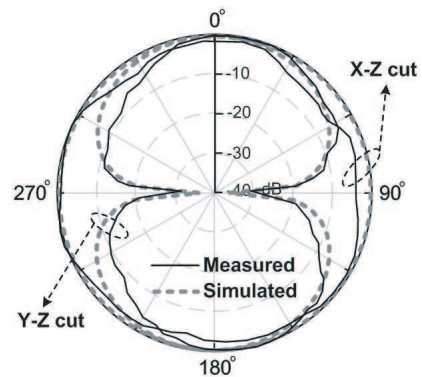


Figure 10. Radiation patterns for 900 MHz.

measured maximum gain was 1.62 dBi for 900 MHz. For polarizations, the AR spectrum is presented in Fig. 11. The minimum AR with 0.25 at $\phi = 0^\circ$, $\theta = 90^\circ$ and the right-hand circular polarizations (-3 dB AR BW = 315 MHz) are observed along the direction of the ϕ and θ , thus the proposed antenna can be applied to circular polarization applications which represents one of the availability and usefulness in contrast to the conventional meander-line and meander-slot tags.

4. CONJUGATE MATCHING PERFORMANCE

For example, the effective transmitted power $EIRP_R$ of reader is 1 W, the sensitivity P_{chip} of tag microchip is -10 dBm, the maximum tag antenna gain $G = 1.62$ dBi, and the activation distance d with boundary condition $d_{1/2} = 2.5/3$ m, the power transmission factor can be obtained $\tau_{1/2} = 0.63/0.91$ by using (1). Then, from (2) and tag antenna impedance ($Z_A = 102.5 + j41.3 \Omega$), the microchip impedance ($Z_{chip} = 16.7 - j45.6 \Omega$) is calculated analytically.

For applications, the variation in antenna impedance, related microchip impedance and tuning pad ($L_t = 1.0, 2.0, 3.0, 4.0$ and 5.0 mm) is shown in Table 1. The varied inductive impedance can be available for matching the related capacitive RFID chip by tuning the pad length. The other example, as the $g = 0.1$ mm, the typical $Z_{chip} = 113 - j167 \Omega$ can be obtained [15].

For deterministic design, the design procedure is stated as: The guided wavelength ($\lambda g/4$) of the central frequency determines the total length of series Hilbert-curve. The desired response and impedance are then tuned by L_t . The final tuning is with g . Using (1) and (2) with boundary condition $d_{1/2}$, the Z_{chip} is obtained. If it is not satisfied, returning L_t and g .

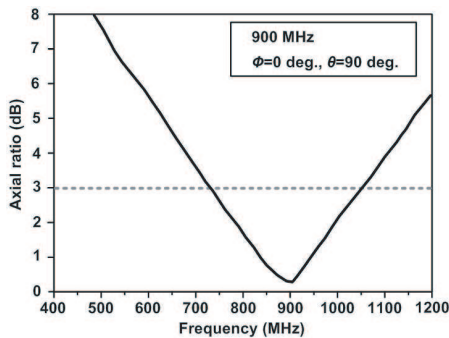


Figure 11. AR spectrum.

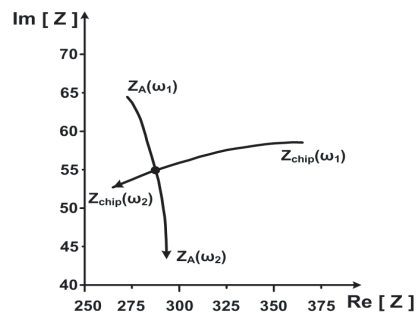


Figure 12. Impedance locus.

Table 1. Variation results (900 MHz).

L_t (mm)	Z_A (Ω)	G_{\max} (dB)	$d_{1/2}$ (m)	$\tau_{1/2}$	Z_{chip} (Ω)
1	97.8 + j46.3	0.98	2.5/3	0.73/1.06	17.6 - j43.4
2	98.7 + j45.6	1.12	2.5/3	0.72/1.03	16.9 - j45.8
3	97.3 + j44.2	1.21	2.5/3	0.7/1.0	17.3 - j42.1
4	99.6 + j43.4	1.38	2.5/3	0.67/0.97	18.9 - j44.8
5	102.5 + j41.3	1.62	2.5/3	0.63/0.91	16.7 - j45.6

A microchip, RI-UHF-STRAP-08 of Texas Instruments, is also used for applications. The diagram of complex plane $Z(\omega)$ is presented in Fig. 12. The microchip impedance locus $Z_{chip}(\omega)$ is firstly plotted in the complex plane. The arrowhead attached to the locus indicates the direction of increasing ω from 860 to 960 MHz. Then, tuning the length, as $g = 0.45$ mm, $L_f = 5.8$ mm and $L_t = 6.3$ mm, the antenna impedance locus $Z_A(\omega)$ is obtained when this ω value is still in the UHF RFID band. The intersection of these two loci corresponds to the operating point, $Z_{chip} = 287 - j55 \Omega$ and $Z_A = 287 + j55 \Omega$.

5. CONCLUSION

The self-complementary antenna with Hilbert-curve configuration for RFID UHF-band tags is presented in this paper. The good performance of compact, broadband (BW = 115 MHz), circular polarization and conjugate impedance matching are achieved for applications. The structure is smaller in size and easy to fabricate in tag circuits. Its operations cover UHF-bands 820 to 935 MHz for return loss < -10 dB. Both simulation and measurement results are agreed with the verified frequency responses. The inductive impedance is achieved and be available for matching the capacitive RFID chip.

In field analysis, conical patterns are observed at broadside in the Y-Z cut and quasi-omnidirectional patterns are obtained in the X-Z cut. The measured maximum gain was 1.62 dBi for 900 MHz. The circular polarization (-3 dB AR BW = 315 MHz) feature of radiation patterns for 900 MHz are presented. There are not much RFID tags using circularly polarization with the advantages of using a CP tags. It is a compact and available CP tag antenna for UHF RFID applications.

ACKNOWLEDGMENT

This research gratefully acknowledges the Industrial Technology Research Institute with Contract No. F650000134.

REFERENCES

1. Lee, H. F. and W. Chen, *Advances in Microstrip and Printed Antennas*, Ch. 4, John Wiley & Sons, Inc. 1997.
2. Marrocco, G., "Gain-optimized self-resonant meander line antennas for RFID applications," *IEEE Antennas Wireless Propag. Lett.*, Vol. 2, 302–305, 2003.
3. Keskilammi, M. and M. Kivikoski, "Using text as a meander line for RFID transponder antennas," *IEEE Antennas Wireless Propag. Lett.*, Vol. 3, 372–374, 2004.
4. Ukkonen, L., L. Sydanheimo, and M. Kivikoski, "Effects of metallic plate size on the performance of microstrip patch-type tag antennas for passive RFID," *IEEE Antennas Wireless Propag. Lett.*, Vol. 4, 410–413, 2005.
5. Son, H. W. and C. S. Pyo, "Design of RFID tag antennas using an inductively coupled feed," *Electron. Lett.*, Vol. 41, No. 18, 994–996, Sep. 2005.
6. Rao, K. V. S., P. V. Nikitin, and S. F. Lam, "Antenna design for UHF RFID tags: A review and a practical application," *IEEE Trans. on Antennas and Propagat.*, Vol. 53, No. 12, 3870–3876, Dec. 2005.
7. Ukkonen, L., M. Schaffrath, D. W. Engels, L. Sydanheimo, and M. Kivikoski, "Operability of folded microstrip patch-type tag antenna in the UHF RFID bands within 865–928 MHz," *IEEE Antennas Wireless Propag. Lett.*, Vol. 5, 414–417, 2006.
8. Chang, C. C. and Y. C. Lo, "Broadband RFID tag antenna with capacitively coupled structure," *Electron. Lett.*, Vol. 42, No. 23, 1322–1323, Nov. 2006.
9. Son, H. W., G. Y. Choi, and C. S. Pyo, "Design of wideband RFID tag antenna for metallic surfaces," *Electron. Lett.*, Vol. 42, No. 5, 263–265, Mar. 2006.
10. Ahn, J., H. Jang, H. Moon, J. W. Lee, and B. Lee, "Inductively coupled compact RFID tag antenna at 910 MHz with near-isotropic radar cross-section (RCS) patterns," *IEEE Antennas Wireless Propag. Lett.*, Vol. 6, 518–520, 2007.
11. Hu, S., C. L. Law, and W. Dou, "Petaloid antenna for passive

- UWB-RFID tags,” *Electron. Lett.*, Vol. 43, No. 22, 1174–1176, Oct. 2007.
12. Vemagiri, J., M. Balachandran, M. Agarwal, and K. Varahramyan, “Development of compact half-sierpinski fractal antenna for RFID applications,” *Electron. Lett.*, Vol. 43, No. 22, 1168–1169, Oct. 2007.
 13. Kim, K. H., J. G. Song, D. H. Kim, H. S. Hu, and J. H. Park, “Fork-shaped RFID tag antenna mountable on metallic surfaces,” *Electron. Lett.*, Vol. 43, No. 23, 1400–1402, Dec. 2007.
 14. Olsson, T., M. Hjelm, J. Siden, and H. E. Nilsson, “Comparative robustness study of planar antenna,” *IET Microw. Antennas Propagat.*, Vol. 1, No. 3, 674–680, Jun. 2007.
 15. Marrocco, G., “RFID antennas for the UHF remote monitoring of human subjects,” *IEEE Trans. on Antennas and Propagat.*, Vol. 55, No. 6, 1862–1870, Jun. 2007.
 16. Calabrese, C. and G. Marrocco, “Meandered-slot antennas for sensor-RFID tags,” *IEEE Antennas Wireless Propag. Lett.*, Vol. 7, 5–8, 2008.
 17. Kim, J.-S., W.-K. Choi, and G.-Y. Choi, “Small proximity coupled ceramic patch antenna for UHF RFID tag mountable on metallic objects,” *Progress In Electromagnetics Research C*, Vol. 4, 129–138, 2008.
 18. Loo, C. H., K. Elmahgoub, F. Yang, A. Elsherbeni, D. Kajfez, A. Kishk, T. Elsherbeni, L. Ukkonen, L. Sydanheimo, M. Kivikoski, S. Merilampi, and P. Ruuskanen, “Chip impedance matching for UHF tag antenna design,” *Progress In Electromagnetics Research*, PIER 81, 359–370, 2008.
 19. Monti, G., L. Catarinucci, and L. Tarricone, “Compact microstrip antenna for RFID applications,” *Progress In Electromagnetics Research Letters*, Vol. 8, 191–199, 2009.
 20. Mushiake, Y., “Self-complementary antennas,” *IEEE Antennas Propagat. Mag.*, Vol. 34, No. 6, 23–29, Dec. 1992.
 21. Mushiake, Y., “A report on Japanese developments of antennas from Yagi-Uda antenna to self-complementary antennas,” *IEEE Antennas Propagat. Mag.*, Vol. 46, No. 4, 47–60, Aug. 2004.
 22. Xu, P., K. Fujimoto, and S. Lin, “Performance of quasi-self-complementary antenna using a monopole and a slot,” *Proc. IEEE Int. Symp. Antennas and Propagation*, Vol. 2, 464–477, 2002.
 23. Xu, P. and K. Fujimoto, “L-shape self-complementary antenna,” *Proc. IEEE Int. Symp. Antennas and Propagation*, Vol. 3, 95–98, 2003.

24. Mosallaei, H. and K. Sarabandi, "A compact ultra-wideband self-complementary antennas with optimal topology and substrate," *Proc. IEEE Int. Symp. Antennas and Propagation*, Vol. 2, 1859–1862, 2004.
25. Saitou, A., T. Iwaki, K. Honjo, K. Sato, T. Koyama, and K. Watnabe, "Practical realization of self-complementary broadband antenna on low-loss resin substrate for UWB applications," *Proc. IEEE MTT-S*, 1265–1268, 2004.
26. Wong, K. L., T. Y. Wu, S. W. Su, and J. W. Lai, "Broadband printed quasi-self-complementary antenna for 5.2/5.8 GHz operation," *Microwave Opt. Tech. Lett.*, Vol. 39, No. 6, 495–496, Dec. 2003.
27. Chen, W. S., C. T. Chang, and K. Y. Ku, "Printed triangular quasi-self-complementary antennas for broadband operation," *Proc. 2007 Int. Symp. Antennas and Propagation*, 262–265, 2007.
28. Sagan, H., *Space-filling Curves*, Springer-Verlag, New York, 1994.
29. Anguera, J., C. Puente, and J. Soler, "Miniature monopole antenna based on the fractal Hilbert curve," *Proc. IEEE Int. Symp. Antennas and Propagation*, Vol. 4, 546–549, 2002.
30. Best, S. R. and J. D. Morrow, "The effectiveness of space-filling fractal geometry in lowering resonant frequency," *IEEE Antennas Wireless Propag. Lett.*, Vol. 1, 112–115, 2002.
31. Yang, X. S., B. Z. Wang, and Y. Zhang, "Two-port reconfigurable Hilbert curve patch antenna," *Microwave Opt. Tech. Lett.*, Vol. 48, No. 1, 91–93, Jan. 2006.
32. HFSS version 10.0, Ansoft Software Inc., 2006.